UAV-UGV cooperative targeted spraying system for honey pomelo orchard

Yuli Chen[1,2,3,4,5,6], Zibo Liu[1,2,3,4,5,6], Zhen Lin[1,2,3,4,5,6], Zifeng Xu[1,2,3,4,5,6], Xianlu Guan[1,2,3,4,5,6], Zhiyan Zhou[1,2,3,4,5,6,9*], Dateng Zheng[7,8], Andrew Hewitt[9]

(1. *College of Engineering, South China Agricultural University and Guangdong Laboratory for Lingnan Modern Agriculture , Guangzhou 510642, China*;
2. *Guangdong Provincial Key Laboratory of Agricultural Artificial Intelligence (GDKL-AAI) , Guangzhou 510642, China*;
3. *Guangdong Engineering Research Center for Agricultural Aviation Application (ERCAAA), Guangzhou 510642, China*;
4. *Key Laboratory of Key Technology on Agricultural Machine and Equipment (South China Agricultural University), Ministry of Education, Guangzhou 510642, China*;
5. *State Key Laboratory of Agricultural Equipment Technology, Guangzhou 510642, China*;
6. *Key Technology Innovation Research Center of Rice Smart Farming of South China Agricultural University - Dongyuan County, Heyuan City 517554, China*;
7. *Institute of Mechanical and Electrical Technology, Jinggangshan University, Ji'an, Jiangxi 343009, China*;
8. *Jiangxi Provincial Key Laboratory of Modern Agricultural Equipment, Ji'an, Jiangxi 343009, China*;
9. *The Centre for Pesticide Application and Safety (CPAS), School of Agriculture and Food Sciences, the University of Queensland, Gatton, QLD 4343, Australia*)

Abstract: To enhance adaptability in orchards with taller average tree heights and improve spraying effectiveness on Jinggang pomelo trees, this paper proposes a UAV-UGV cooperative targeted spraying system (UCTSS) and develops a prototype. The UCTSS primarily consists of a UAV and a UGV, networked using the Robot Operating System (ROS). During operation, both the UAV and UGV navigate between tree rows while carrying the spraying module. When the UAV reaches suitable spraying positions, the UGV halts to activate the spraying module, and the UAV performs targeted spraying from top to bottom. The paper employs a master-slave method for basic formation control of the UAV and UGV, resulting in an average tracking error of 0.118 m and a standard deviation of 0.040 m during testing. Additionally, a LiDAR-based targeted spraying detection method is designed and validated through simulation experiments, achieving an accuracy rate of 96% with an average position error of 0.13 m. Field trials in orchards demonstrate that the UCTSS meets stability requirements, with the average tracking error of the UAV measuring 0.158 m during coordinated movement and 0.013 m during spraying. In terms of spraying effectiveness, the UCTSS exhibits higher average droplet density and deposition values at various heights of the same tree compared to the DJI-T50, along with a lower coefficient of variation between levels, resulting in a more uniform spraying effect. The feasibility of the UCTSS is validated, providing a novel approach for orchard protection in areas with taller average tree heights.

Keywords: plant protection, UAV-UGV cooperation, orchard, master-slave, targeted spraying, LiDAR
DOI: 10.25165/j.ijabe.20241706.8989

Citation: Chen Y L, Liu Z B, Lin Z, Xu Z F, Guan X L, Zhou Z Y, et al. UAV-UGV cooperative targeted spraying system for honey pomelo orchard. Int J Agric & Biol Eng, 2024; 17(6): 22–31.

1 Introduction

In orchard management, plant protection is crucial for ensuring the stability and yield of fruit production, accounting for approximately 30% of the total workload[1,2]. Previous research on unmanned plant protection in orchards can be categorized into two areas: ground-based spraying machinery and plant protection drones.

In addition, to improve the pesticide utilization and the spraying effects for the hilly orchard, these methods and techniques are applied to ground orchard sprayers: air-assisted spraying technology[3-5], electrostatic spraying technology[6-8], tunnel spraying technology[9,10], variable rate spraying technology[11-14], profiling spray technology[15,16], etc. Researchers have integrated one or more of these technologies into a single sprayer.

Compared with ground spray machinery, UAVs (unmanned air vehicles) for rotor plant protection are less affected by the terrain and have the advantage of high flexibility. UAVs for rotor plant protection have also become an important method of plant protection in orchards in recent years[17]. But due to the limitation of their endurance and the amount of pesticides they carry, their work efficiency is limited to a certain extent. In contrast, the ground sprayer has greater pesticide storage capacity and endurance.

Received date: 2024-04-10 **Accepted date:** 2024-10-22
Biographies: **Yuli Chen**, PhD candidate, research interest: multi-robot cooperation, Email: chenyuliii@foxmail.com; **Zibo Liu**, MC candidate, research interest: agricultural artificial intelligence technology, Email: 2095442787@qq.com; **Zhen Lin**, MC candidate, research interest: plant protection UAV, Email: 735020349@qq.com; **Zifeng Xu**, MC candidate, research interest: Tethered energy supply, Email: xuzifeng@stu.scau.edu.cn; **Xianlu Guan**, PhD candidate, research interest: multi-robot cooperation, Email: guanxl@stu.scau.edu.cn; **Dateng Zheng**, PhD, Professor, research interest: Intelligent agricultural machinery control system, Email: yizh9026@163.com; **Andrew Hewitt**, PhD, Professor, research interest: Pesticide Application and Safety, Email: a.hewitt@uq.edu.au.

***Corresponding author: Zhiyan Zhou**, PhD, Professor, research interest: Agricultural artificial intelligence technology, College of Engineering, South China Agricultural University, Guangzhou 510642, China, Tel: +86-20-38676975, Email: zyzhou@scau.edu.cn.

In recent years, there has been considerable research on the application of UAV-UGV cooperation systems in various fields such as transportation, rescue operations, and agriculture. Many scholars have employed UAVs as actuators and UGVs (unmanned ground vehicles) as mobile carriers, addressing issues such as UAV landing during UGV stationary position or movement using methods like deep learning[18], reinforcement learning[19], and computer vision[20,21]. These approaches have been applied in scenarios like parcel delivery, where UAVs, leveraging UGVs' endurance and payload capacity, transport goods close to the target for last-mile delivery. Researchers have also investigated problems related to path planning and task allocation in this context. Additionally, some scholars have utilized UAVs as sensors and UGVs as actuators, leveraging UAVs' mobility to gather environmental data for UGV navigation assistance. In the agricultural domain, Li et al.[22] introduced a method employing UAV and UGV collaboration for mango tree spraying, which outperformed single machinery in spraying operations. Similarly, Tokelar et al.[23] optimized UAV-UGV cooperation systems to reduce UAV flight distance and energy consumption for soil measurements. Zhang et al.[24] proposed a precise pesticide spraying system based on UAV-UGV cooperation in agriculture, in which UAVs are equipped with remote sensing devices to detect pests and diseases over a large area in farmlands. The detection results are then transmitted to UGVs, which autonomously navigate to the locations of crops affected by pests and diseases. They then conduct secondary inspections using methods such as machine vision and complete pesticide spraying. Tevel, an Israeli company, developed a fruit-picking robot based on UAV-UGV cooperation, in which multiple UAVs equipped with picking devices and depth cameras are used to identify, locate, and pick fruits. A UGV provides power to these UAVs and collects the fruits picked by them. This robot system can complete fruit-picking tasks ranging from a 50 g (2 oz) apricot to a 700 g (25 oz) apple in standard orchards.

In the economically important Jinggang pomelo crop, unique to Ji'an City, Jiangxi Province, China, the foliage area of the fruit trees is relatively large compared to regular pomelo trees, with rigid branches and denser canopies. During its growth stage, a spraying device that can flexibly adjust the spraying range is required to compensate for the poor droplet uniformity when solely using agricultural drones for spraying operations.

To overcome the limitations described above, this paper proposes a UAV-UGV cooperative targeted spraying system, referred to as UCTSS. This system introduces a novel approach to orchard spraying, effectively carrying out operations in orchards with taller average tree heights. Additionally, a cooperative control algorithm and a LiDAR-based targeted spraying detection method have been developed, enabling the coordinated movement of drones and unmanned vehicles to efficiently complete orchard spraying. Finally, the feasibility of the UCTSS was verified through field tests.

2 Materials and methods

2.1 System description

The UCTSS proposed in this paper, as depicted in Figure 1, primarily consists of a UAV and a UGV. The UAV is equipped with an arc-shaped spray boom for conducting spraying operations on fruit trees, while the UGV carries heavy equipment, including batteries, pesticide tanks, hose reels, pumps, and other components. These components supply power to both the UGV and the UAV, as well as provide pesticide and spray pressure support.

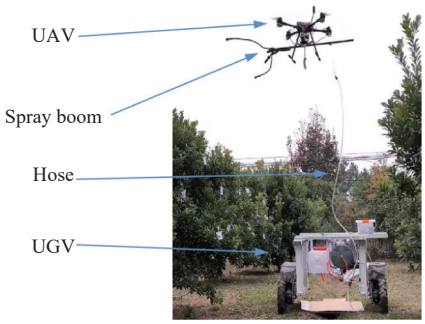

Figure 1 Structure of the UCTSS

The main technical parameters of the prototype of the UCTSS are listed in Table 1.

Table 1 Main technical parameters

Parameters	Values
UGV Boundary dimension/m	1.2×1.5×1.2
UGV Driving speed/m·s^{-1}	0-0.5
UGV Empty mass/kg	200
UAV Diagonal wheelbase/mm	680
UAV Operating Payload/kg	3.5
UAV Lifting range with sprayer/m	1.5-5.5
Liquid volume/L	50
Spraying power/kW	0.2
Theoretical spraying volume/L·min^{-1}	8-10

Regarding the control-related components of the UCTSS, as shown in Figure 2 below, both the UAV and UGV are equipped with autopilots, onboard computers, and RTK (Real-Time Kinematic) system. The autopilot firmware used is Pixhawk, serving as the lower-level controller, while ROS is installed on the onboard computer, acting as the upper-level controller. Additionally, a router is installed on the UGV to establish a ROS network, facilitating data transmission between the UAV and UGV, as well as a pump for controlling the start and stop of the spraying action.

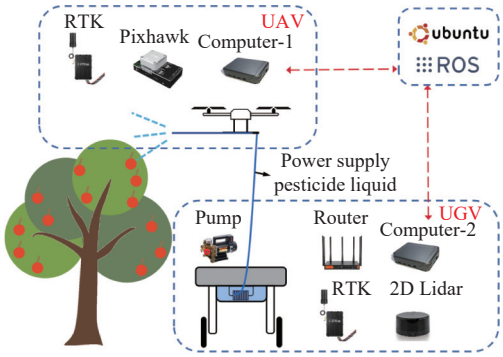

Figure 2 Control composition of the UCTSS

The relevant parameters of the involved sensors and control components are listed in Table 2.

Table 2 Parameters of the sensors and control components

Sensor/Control component	Version/Model/Accuracy
Autopilots	CUAV V5+
Firmware	PX4-V1.12.3
RTK	CUAV 9Ps/0.01 m+1 ppm CEP
Onboard computer	Raspberry Pi 4B(8 g)
ROS	Noetic
LiDAR	LeiShen-M10P

2.2 Working principle

2.2.1 Working process of the UCTSS

Taking the spraying process of the UCTSS on a single tree as an example, it can be divided into three stages:

Through the spraying process illustrated in Figure 3, which involves UAV-UGV formation control and the targeted spraying detection method, this paper will elaborate on these topics in Sections 2.2.2 and 2.2.3. Below is a specific description of the three steps in the spraying process. In this description, the UAV is positioned directly above the UGV to illustrate the formation; however, in practice, the UAV's position within the formation can vary based on the specific work environment, while the spraying process remains consistent.

To conveniently describe the spraying process of the UCTSS, an ideal local coordinate system *O*-*XYZ* is established, as shown in Figures 4-6. It is important to emphasize that this coordinate system is used solely for explaining the spraying process, and the actual operation does not involve movement along a single axis.

During the formation driving stage, the expected position of the UAV in the *X*-*Y* plane is set to match the position of the UGV, while the desired flight height of the UAV is determined based on the height of the UGV and the average height of the orchard trees, as elaborated in the following section. In this description, the (x, y) coordinates of the UGV and UAV are expected to remain consistent, with both moving in a fixed formation in the *Y*-direction.

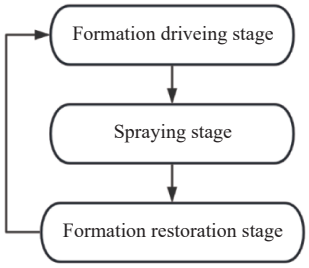

Figure 3 Workflow of the UCTSS

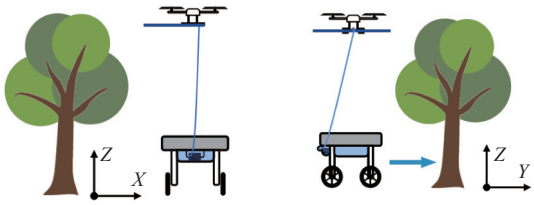

a. Rear view b. Right view

Figure 4 Formation driving stage

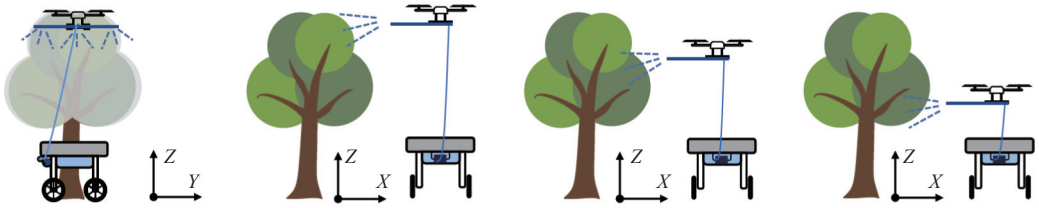

a. Right view b1. Rear view-1 b2. Rear view-2 b3. Rear view-3

Figure 5 Spraying stage

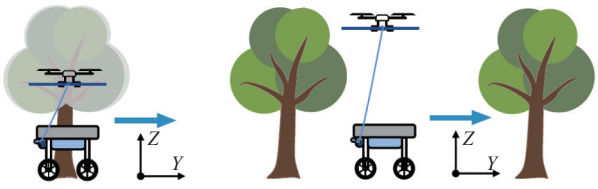

a. Right view b. Right view

Figure 6 Formation restoration stage

Since the orchard is not located on flat terrain, the real-time relative height of the UGV's position is denoted as z_0. When the height at which the UGV begins operation is initialized to 0, z_0 is equivalent to the relative height of the ground on which the UGV is situated. Let the height of the UAV within the formation be denoted as z_2; thus, during the formation driving stage, the UAV's expected flight height is z_0+z_2.

The UGV is equipped with LiDAR, which continuously scans the surroundings as the UCTSS moves. As shown in Figure 5a, when the detection algorithm identifies that the UGV has reached the ideal spray position in front of the fruit tree, the spraying process is initiated, as illustrated in Figures 5b1-5b3.

Figures 5a and 5b1-5b3 represent the right view and rear view respectively when the UGV has reached the ideal spray position in front of the fruit tree. Subsequently, Figures 5b1-5b3 illustrate the process in which the UAV, equipped with a spray boom, moves uniformly from top to bottom, completing the targeted spraying of orchard trees from the side. Using the real-time height of the UGV as a reference, z_2 denotes the UAV's flight height during formation (as shown in Figure 5b1), and z_3 denotes the UAV's height when spraying stops (as shown in Figure 5b3). The specific description of the spraying stage of the UCTSS is as follows:

(1) When the UCTSS determines that the UGV has reached the target spraying position based on the LiDAR return values, it records the UGV's coordinates in the *X*-*Y* plane as (x_s, y_s). The UAV's expected position in the *X*-*Y* plane is then updated to (x_s, y_s) rather than the UGV's current position. This ensures that even if the UGV's position changes during the spraying process, the UAV's spraying accuracy remains unaffected.

(2) Once the UAV reaches (x_s, y_s), the UGV immediately stops moving, and the spraying unit is activated to begin spraying. Simultaneously, the UAV moves vertically downward at a speed of 0.3 m/s, lowering from z_0+z_2 to z_0+z_3, completing the spraying on the side of the fruit tree.

(3) After the UAV's height reaches z_0+z_3, the spraying unit is turned off, and the UAV ascends at a speed of 0.5 m/s until it reaches the height of z_0+z_2. During this time, the UAV's expected position in the *X*-*Y* plane is updated to match the real-time position of the UGV in the formation, allowing both the UAV and UGV to continue moving along the pre-planned path, as shown in Figure 6.

(4) When the Euclidean distance between the UGV's real-time position in the *X*-*Y* plane and (x_s, y_s) from the previous spraying stage exceeds 0.8*R, the UCTSS begins using LiDAR return values to determine if the UGV has reached the next target spraying position.

2.2.2 UAV-UGV formation control

According to the operation process of the UCTSS outlined in the previous section, the cooperative control method designed in this paper needs to meet the following requirements:

(1) When the UCTSS moves between rows of fruit trees, the UAV and UGV in the system perform formation movement in the ENU coordinate system, advancing smoothly to minimize the sway of the hose.

(2) When the UCTSS is spraying fruit trees, the UGV stops at the position identified for targeted spraying by LiDAR, while the UAV aims to maintain the same position. The spraying is conducted from top to bottom on the side of the fruit tree. At this moment, any tracking error directly affects both the effectiveness of the spraying and the targeting accuracy.

The master-slave (also known as leader-follower) cooperation mode is one of the most effective control methods in the field of multi-machine collaboration[25-27]. In this paper, a cooperative control algorithm was developed for UAV and UGV based on the master-slave cooperation framework. Given the greater flexibility of UAV compared to UGV, the UGV is selected as the master and the UAV as the slave within this system. Position control of the UAV and UGV is achieved by controlling their linear velocity and angular velocity. The master's control is not influenced by the slave; instead, it is governed solely by the desired route and its own status feedback. The UGV utilizes a four-wheel differential drive chassis, which features a small turning radius, providing better maneuverability in orchards[28]. The kinematic model of this type of chassis is as follows:

$$\begin{bmatrix} v_0 \\ w_0 \end{bmatrix} = \begin{bmatrix} \frac{1}{2} & \frac{1}{2} \\ \frac{1}{2L_0} & -\frac{1}{2L_0} \end{bmatrix} \cdot \begin{bmatrix} v_l \\ v_r \end{bmatrix} \tag{1}$$

where, v_0 and w_0 represent the linear velocity and angular velocity of the UGV, respectively; v_l and v_r represent the linear velocities of the left and right wheels, respectively; and L_0 represents the wheelbase of the UGV.

The kinematic model of the UAV (quadcopter) is as follows:

$$\begin{bmatrix} \dot{x}_1 & \dot{y}_1 & \dot{z}_1 & \dot{\theta}_1 \end{bmatrix}^{\mathrm{T}} = \begin{bmatrix} v_{x1} & v_{y1} & v_{z1} & \omega_1 \end{bmatrix}^{\mathrm{T}} \tag{2}$$

where, x_1, y_1, and z_1 are the displacements of the UAV in the eastern, northern, and perpendicular to the ground direction of the NEU coordinate system, respectively; θ is the yaw of the UAV; and ω_1 is the yaw angular velocity of the UAV.

Before the UCTSS initiates formation movement, the flight altitude of the UAV is initially set based on the average height of fruit trees within the orchard. The initial flight height of the UAV in this paper is set as H+1, where H represents the average height of fruit trees in standard orchards. The real-time relative height of the UGV can be measured by RTK and recorded as z_0. In the process of UGV motion, the height value of its position will vary with the changes in the orchard ground height. Therefore, the height of the UAV in the formation driving stage is set as H+z_0+1; this value corresponds to the "z_2" previously mentioned in this paper.

Subsequently, the UAV and UGV begin to move forward together. A top view of the process is shown inFigure 7.

As shown in Figure 7, within the E-N coordinate system, point A_r represents the current position of the UAV, and point G signifies the position of the UGV. The angle α corresponds to the planned heading of the UCTSS, while m signifies the distance between the UAV and UGV in the formation. The expected position of the UAV within the formation is denoted as A_v and is characterized by the corresponding (x, y) coordinates. The positions of points A_r and G can be determined through sensors, and point A_r can be expressed as:

$$\begin{bmatrix} x_v \\ y_v \\ z_v \end{bmatrix} = \begin{bmatrix} x_g \\ y_g \\ z_g + H + 1 \end{bmatrix} - m \cdot \begin{bmatrix} \sin\alpha \\ \cos\alpha \\ 0 \end{bmatrix} \tag{3}$$

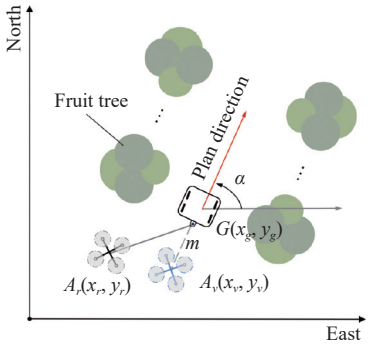

Figure 7 Schematic diagram of coordinated progress

The yaw of the UAV can be individually closed-loop controlled according to the planned direction. In the E-N-U (East-North-Up) coordinate system, the error model for tracking error of the UAV is as follows:

$$\begin{bmatrix} e_x \\ e_y \\ e_z \end{bmatrix} = \begin{bmatrix} x_v \\ y_v \\ z_v \end{bmatrix} - \begin{bmatrix} x_r \\ y_r \\ z_r \end{bmatrix} = \begin{bmatrix} x_g - x_r \\ y_g - y_r \\ z_g + H + 1 - z_r \end{bmatrix} - m \cdot \begin{bmatrix} \sin\alpha \\ \cos\alpha \\ 0 \end{bmatrix} \tag{4}$$

To achieve control of the position of the UAV with respect to the UGV and maintain formation, a position-velocity control algorithm is employed. This is achieved by controlling the linear velocities of UAV, v_{ax}, and v_{ay}. This paper utilizes a PD (proportional-derivative) controller:

$$\begin{bmatrix} v_{ax} \\ v_{ay} \\ v_{az} \end{bmatrix} = K_P \cdot \begin{bmatrix} e_x \\ e_y \\ e_z \end{bmatrix} + K_d \cdot \begin{bmatrix} v_{gx} - v_{ax} \\ v_{gy} - v_{ay} \\ v_{gz} - v_{az} \end{bmatrix} \tag{5}$$

where, v_{ax} and v_{ay} represent the linear velocities of UAV in the X and Y directions in the ENU coordinate system, while v_{gx} and v_{gy} represent the linear velocities of UGV in the same coordinate system. K_p stands for the proportional gain, which is used to adjust the impact of position error on velocity, and K_d is the derivative gain, used to adjust the impact of velocity error on velocity.

To verify the feasibility of the UAV-UGV collaborative control method described above, the test was conducted on a hard cement road surface. The test site and scenarios are illustrated in Figure 8. The weather on the test day was clear, with temperatures ranging from 28ºC to 34ºC and a wind speed of 2 m/s. During the test, the UGV was pre-planned to move at a constant speed of 0.4-0.5 m/s in a straight line for a distance of 20 m. The UAV followed the UGV in a formation motion, the test focused solely on evaluating the formation control performance without installing the hose and spray boom, and the test was repeated three times. The tracking error of UAV in the E-N coordinate system was calculated by combining Equation (4) and the following Equation (6):

$$E = \sqrt{e_x^2 + e_y^2} \tag{6}$$

Based on the test results, the average tracking error of the UAV was 0.118 m, with a standard deviation of 0.040 m, meeting the previously stated requirements. The next step involves installing the spraying unit for further experiments.

Figure 8 Formation control test of UAV-UGV

2.3 Targeted spraying detection method

The purpose of targeted spraying is to enhance pesticide utilization[29,30]. The key issue is accurately determining the position of the fruit trees. Currently, methods for achieving this targeting include infrared optical sensors, ultrasonic detection, laser detection, and visual methods. Among these, LiDAR detection is a primary method for identifying tree canopy structures[31-33]. This section will explain how to use LiDAR to determine the ideal spraying position for the UCTSS.

2.3.1 Overview of the spraying position detection process

Based on the working process of the UCTSS described earlier in this paper, navigating to the ideal spraying position on the side of the fruit tree is a crucial step. As shown in Figure 9a illustrates the top view of the UGV driving along the predefined route under ideal conditions. At this point, the range of fruit trees in the plane can be approximated as a circle, with a perpendicular line drawn from the circle's center to the plan direction; the foot point labeled *A* corresponds to the ideal targeted spraying position.

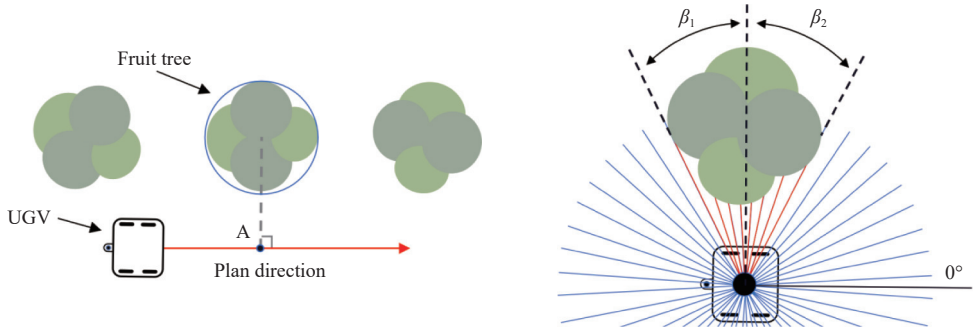

a. The ideal targeted spraying position b. The scanning results from the LiDAR

Figure 9 Diagram of targeted spraying position

On the back of the steel beam atop the UGV, a LiDAR sensor is installed to detect the surrounding environment and generate point cloud data. The purpose of this algorithm is to determine whether the UGV has reached the ideal targeted spraying position as the UCTSS advances in the planned direction, based on the data returned by the LiDAR.

In Figure 9b, the scanning results of the LiDAR after the UGV has reached point *A* are illustrated. In this illustration, the red area represents the scanned region where fruit trees have been detected, while the blue area indicates the region where no fruit trees have been detected. Let the distance between the fruit trees be denoted as L_1. As the UGV travels between the rows, the distances m corresponding to the reflection points of these red beams to the 0° beam satisfy:

$$m \le T_0 \tag{7}$$

where T_0 represents the distance judgment threshold, indicating the maximum value of m among the red beams in Figure 9b. If the m value corresponding to a beam is less than or equal to T_0, it can be determined that the beam is within the range of the fruit tree canopy.

Let n_1 and n_2 represent the number of red beams within the β_1 and β_2 regions, respectively.

$$\begin{bmatrix} \beta_1 \\ n_1 \end{bmatrix} = \begin{bmatrix} \beta_2 \\ n_2 \end{bmatrix} \tag{8}$$

At this point, the total number of beams in the red area of the LiDAR is denoted as N_0:

$$N_0 = n_1 + n_2 \tag{9}$$

The number of points n_1 and n_2 within the range of the fruit tree in the point cloud data returned by LiDAR satisfies:

$$\begin{cases} n_1 + n_2 = N_0 \\ |n_1 - n_2| = 0 \end{cases} \tag{10}$$

Conversely, if n_1 and n_2 satisfy Equation (10), it can be concluded that the UGV has reached point *A*, which represents the ideal targeted spraying position.

2.3.2 Design and simulation of the spraying position detection method

In practical standardized orchards, irregular gaps in the fruit tree canopy may render Equations (8) and (10) invalid. To investigate the relationship between n_1 and n_2 in such scenarios, a simulation environment was created in Gazebo to emulate real fruit trees, as shown in the following figure.

As observed from Figure 10, due to the presence of numerous irregular gaps in the canopy, some laser beams pass through the gaps between leaves, resulting in noise. Therefore, a sliding minimum value filter is used to filter the point cloud data, with the aim of retaining only the outline information of the outer layer of the tree canopy, eliminating the influence of gaps between leaves on the LiDAR. Define a new sequence y, where $y_{[i]}$ represents the minimum value within a sliding window starting at $x_{[i]}$. The size of the sliding window is set to j, so for $y_{[i]}$, the calculation formula is as follows:

$$y_{[i]} = \min(x_{[i]}, x_{[i+1]}, x_{[i+2]} \ldots, x_{[i+j]}) \tag{11}$$

where $x_{[i]}$ to $x_{[i+j]}$ represents the elements in the x sequence from index i to index $i+j$.

Using the method described above, point cloud data in each time dimension is filtered with a sliding window of size 10 (the size of the sliding window should be determined based on the observed

gaps between fruit tree crowns and the point cloud density) and a step size of 1. The original point cloud data is transformed into a new sequence y. Two fruit trees were selected to collect crown contour information, and a comparison of the point cloud data before and after filtering is illustrated in Figure 11.

After the aforementioned filtering process, the LiDAR point cloud data within the tree canopy exhibits improved integrity and continuity. To minimize the influence of adjacent trees on the point cloud results, the range of LiDAR data collection can be reduced.

This study sets the LiDAR single-sided point cloud collection range to [225°, 270°) as an example, and outlines the following steps to determine whether the UGV has reached an appropriate spraying position:

(1) Calculate the distance of each point in the filtered data to the 0° beam, obtaining sequence m. Count the number of points in sequence m that are less than or equal to T_0 within the ranges [225°, 270°) and [270°, 315°), denoted as n_1 and n_2, respectively;

(2) Determine whether s satisfies the following condition:

$$s > 0.8R \tag{12}$$

3) Determine whether n_1 and n_2 satisfy the following condition:

$$\begin{cases} n_1 + n_2 \geq T_1 \\ |n_1 - n_2| \leq T_2 \end{cases} \tag{13}$$

where, T_1 and T_2 are the threshold values used to replace N_0 and 0 in Equation (10), respectively. They are used to assess whether the number and distribution of points in the filtered point cloud that meet the criteria in Equation (7) correspond to the point cloud characteristics of an individual fruit tree.

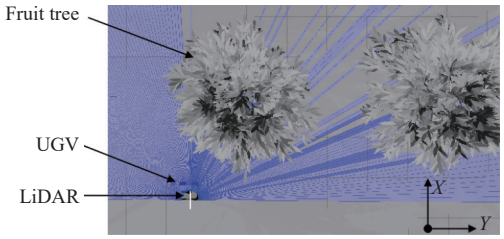

Figure 10 Simulation environment

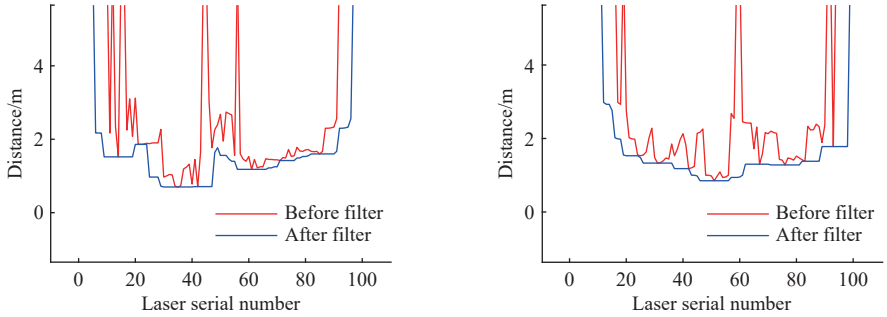

Figure 11 Comparison schematic diagram before and after filtering

As shown in Figure 12a, Equation (13) holds in this case, but the expected position has not been reached. To avoid such situations, first determine whether Equation (12) is satisfied, and then check if Equation (13) is met.

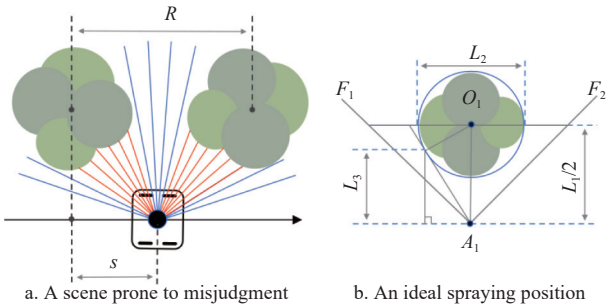

a. A scene prone to misjudgment b. An ideal spraying position scene

Note: S is the Euclidean distance between the real-time position of the UGV and the previous spraying position; R is the distance between fruit trees; L_1 is the row spacing of the fruit trees; L_2 is the diameter of the fruit trees; O_1 is the ideal center point of the fruit tree; and A_1 is the ideal spraying position.

Figure 12 Two LiDAR detection conditions

In Figure 12b, if the fruit tree is considered as a regular circle, the minimum value that T_0 can take in Equation (7) is L_3. However, since the external contour of the fruit tree is not a regular circle and there are irregular gaps in the canopy, T_0 should be taken as a constant greater than L_3:

$$T_0 = 0.65L_1 \tag{14}$$

The LiDAR beams are uniformly distributed within the circular area. If the effects of UGV lateral movement, vibrations, and other factors during travel are not considered, T_1 can be taken as:

$$T_1 = N_1^r \cdot \left[4\arcsin\left(L_{2\min}/L_1\right)/\pi + p\right] \tag{15}$$

where, n represents the total number of actual beams within the range [225°, 270°); r denotes the minimum radius of the fruit tree; and p is an additional constant, which is a negative value.

When the UGV is at point A_1, in an ideal scenario, the circle representing the fruit tree is symmetric about the line O_1A_1, making Equation (10) valid. However, considering that the actual external contour of the fruit tree is irregular and factors such as sensor collection frequency, T_2 should be increased appropriately.

$$T_2 = 0.02N_1^r \tag{16}$$

When $|n_1 - n_2| \leq T_2$ holds, it indicates that the circle representing the fruit tree is symmetric about line O_1A_1. If $n_1 + n_2 \geq T_1$ also holds at this time, it is considered that the UGV has reached the ideal spraying position.

In the simulation environment, fruit trees are considered as circles in the X-Y plane, making it relatively easier to estimate the center position compared to the actual environment. The ideal spraying position (x_3, y_3) can then be calculated. Various methods are employed to compute n_1 and n_2, and each time the UGV's parking position (x_4, y_4) is recorded. The error is calculated as follows:

$$E_1 = \sqrt{(x_3 - x_4)^2 + (y_3 - y_4)^2} \tag{17}$$

Using the aforementioned targeted spraying position detection method, simulation experiments were conducted in the Gazebo simulation environment. The UGV was maneuvered between virtual fruit trees, and LiDAR feedback was utilized to determine if the UGV had reached the targeted spraying position. Ten experiments were conducted in an environment with a total of five virtual fruit trees, each time slightly altering the angle of the trees along the *Z*-axis. If the targeted spraying position algorithm on the ROS topic returned "True" when passing through a virtual fruit tree, it was considered effective, and the UGV's position was recorded. Conversely, if the algorithm consistently did not return "True" when passing through a virtual fruit tree, it was deemed ineffective. Ultimately, the success rate of targeted spraying position detection was determined to be 96%, with an average error E_1 of 0.13 m, meeting the operational requirements for targeted spraying. Further experiments can be conducted based on these results.

2.4 Orchard experiment design

The experiment was conducted on November 26, 2023, at the JingGang Pomelo Standardization Demonstration Base in Ji'an City, Jiangxi Province, China. The weather was clear, with temperatures ranging from 16ºC to 20ºC and a wind speed of 2-3 levels. Three consecutive trees were selected, and for each tree, 15 sampling points were evenly distributed at the upper, middle, and lower levels on one side of each plane, as shown in Figure 13.

Following the aforementioned sampling point layout method, due to the dense canopy layer of Jinggang pomelo trees, 15 droplet collection cards were placed approximately 30 to 40 cm inside the outer layer of the canopy.

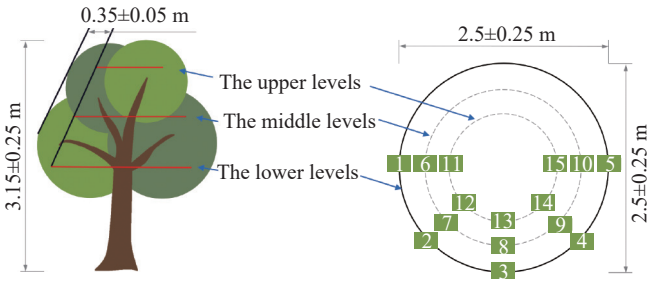

Figure 13 Diagram of label paper layout

The purpose of the experiment is to validate the effectiveness of the UCTSS and its targeted spraying method, specifically to verify the spraying efficacy within the canopy of pomelo trees. To this end, the spraying operations were conducted using the DJI-T50 under the same experimental conditions for comparative analysis of spraying effectiveness. The flight and spraying parameters for the DJI-T50[34] were optimized: the flight altitude was set at 3 m above the top of the canopy, the flight speed was 3 m/s, and the spraying flow rate was 16 L/min. Under these parameter settings, the DJI-T50 demonstrated superior spraying effectiveness in the orchard. The experimental site and spray operation schematic are shown in Figure 14.

a. Experimental site b. Experimental process

Figure 14 Experimental site and schematic diagram of the experimental process

3 Results and discussion

3.1 UAV-UGV formation

The tracking accuracy of the UAV is one of the key factors affecting the stability of the UCTSS and the effectiveness of spraying. In this experiment, as the system sprayed three trees, the tracking errors of the UAV in the E-N coordinate system were calculated by combining Equations (4) and (6). The tracking errors of the UAV were recorded according to this process, as shown in Figure 15.

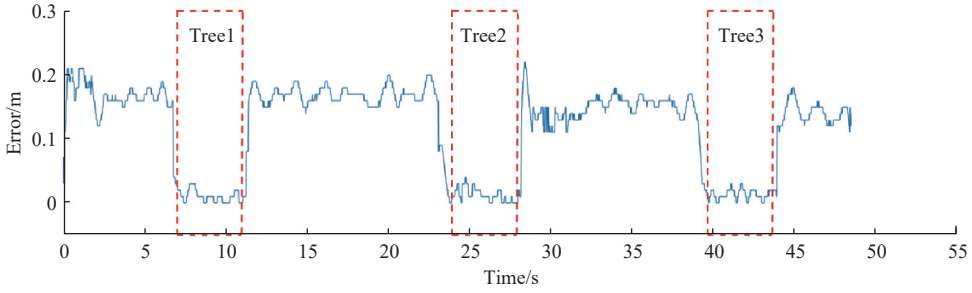

Figure 15 Tracking errors of the UAV

As observed in Figure 15, there are two distinct types of error curves. This phenomenon arises because the tracking targets of the UAV in the E-N coordinate system differ across various operational stages. The relationship between the tracking targets and the operational stages of the UCTSS is listed in Table 3.

Table 3 Tracking targets of the UAV in each stage

UCTSS operational stages	UAV tracking targets
Formation driving stage	Expected position within UAV-UGV formation
Spraying stage	Spraying position
Formation restoration stage	Expected position within UAV-UGV formation

The figure and table above illustrate two states during the coordinated forward movement of the UAV and UGV in the UCTSS:

(1) The curve within the red box describes the error variation of the UCTSS during the spraying stage. During this stage, the expected coordinates of the UAV and UGV remain unchanged in the E-N coordinate system, with the UAV adjusting only its flight altitude for spraying. The average tracking error of the UAV is 0.013 m, the standard deviation is 0.032 m, and the maximum error is 0.06 m.

(2) The curves outside the red box describe the error variations of the UCTSS during the formation driving stage and formation restoration stage. During these two stages, the UGV functions as the leader, moving at a speed of 0.5 m/s to detect trees on the side, while the UAV, acting as the follower, tracks the UGV's position. The average tracking error of the UAV is 0.158 m, the standard deviation is 0.048 m, and the maximum error is 0.21 m.

The tracking error of the UAV during the spraying stage of the UCTSS directly affects the accuracy and effectiveness of the spraying. At this point, the UGV stops moving, and the UAV's tracking target is the spray position detected by LiDAR, which is a fixed point. As indicated earlier, the UAV's following error fluctuates around 0.013 m during this process. The main causes of this fluctuation are the influence of natural wind and the reactive forces generated by changes in the spray boom during the spraying process, leading to a maximum error of 0.06 m. Considering the standard deviation, the UAV exhibits minimal fluctuation near the spray position during the spraying stage, meeting the stability and accuracy requirements of the UCTSS during the spraying process.

Similarly, during the formation driving stage and formation restoration stage of the UCTSS, the UAV's tracking error fluctuates around 0.158 m. At this time, the UAV and UGV are in a formation moving state, with the UAV's tracking target being the expected position within the formation, which is a dynamic point, resulting in relatively larger errors. This formation error does not affect the spraying effectiveness but impacts the stability of the UCTSS during operation. Excessive fluctuations can cause the hose, as shown in Figure 1, to oscillate in the air, compromising the stability of the UCTSS. Considering the standard deviation at this time and observations of the hose during the experiment, the requirements for stability during UCTSS operation are met.

3.2 Spray effectiveness statistics

The sampling substrates were collected only after the droplets had completely dried. The retrieved substrates were labeled and subjected to microscopic photography. The images were then transferred to a computer image analysis system for analysis to calculate the average droplet density for each layer of fruit trees, the average droplet deposition, and their coefficients of variation at the same height level of a single tree, as well as across all height levels. After the experiments concluded, the substrates were allowed to air-dry before collection. Data were then analyzed using the aforementioned method, and the results are listed in Table 4. In the table, "UCTSS" denotes the UAV-UGV cooperative targeted spraying system, while "DJI-T50" represents the statistical analysis of the spraying effect of DJI-T50's agricultural multi-rotor drone under the same experimental conditions.

The coefficient of variation for droplet density and droplet deposition was calculated and statistically analyzed for each individual tree, as well as for each level of the tree. The results are summarized in Table 5.

Table 4 Comparison of different spraying methods

Value	Position	Spraying method	1			2			3			Average
			Upper	Middle	Lower	Upper	Middle	Lower	Upper	Middle	Lower	
Droplet density (droplets·cm^{-2})	Leaf surface	UCTSS	74.6	225.6	93.5	66.5	122.5	68.9	93.5	122.0	72.7	104.4
		DJI-T50	90.9	40.3	16.4	91.7	52.3	42.8	55.8	80.5	47.3	57.5
	Leaf underside	UCTSS	39.2	72.9	29.2	44.3	15.7	21.2	41.70	47.1	32.3	38.2
		DJI-T50	13.8	8.2	1.7	13.5	6.0	4.6	5.5	0.9	6.1	6.7
Droplet deposition (μL·cm^{-2})	Leaf surface	UCTSS	0.782	2.320	0.718	0.869	1.305	0.397	0.395	1.119	0.797	0.967
		DJI-T50	0.343	0.130	0.027	0.361	0.357	0.090	0.161	0.194	0.151	0.203
	Leaf underside	UCTSS	0.044	0.270	0.073	0.134	0.055	0.106	0.073	0.083	0.054	0.099
		DJI-T50	0.019	0.008	0.006	0.018	0.027	0.014	0.008	0001	0.018	0.013

From the average droplet density of three trees, the UCTSS demonstrated higher average droplet densities on both the leaf surface and the leaf underside, with values of 104.4 droplets/cm^2 and 38.2 droplets/cm^2, respectively. In contrast, the T50 showed average droplet densities of 57.5 droplets/cm^2 and 6.7 droplets/cm^2 on the leaf surface and leaf underside, respectively. The same trend was observed for the average droplet deposition. This phenomenon can be attributed to the placement of the UCTSS pump power source and pesticide tank on the UGV, which enhances its endurance. Consequently, the UCTSS can operate at higher voltage and spray pressure, resulting in wider distribution, denser coverage, and better adhesion to the leaf underside.

Examining the average droplet density and droplet deposition at different levels of the same tree, the UCTSS exhibited higher values at the middle levels, with less noticeable differences between the upper and lower levels. In contrast, the T50 showed higher average droplet density and droplet deposition at the upper and middle levels compared to the lower levels. This phenomenon was particularly pronounced in the thick canopy of Jinggang pomelo trees. The T50's operation involves spraying from the top down, causing average droplet density and droplet deposition to decrease as the levels lower. Conversely, the UCTSS sprays from the side, from top to bottom, resulting in less sensitivity to tree height. However, due to the overall spherical shape of Jinggang pomelo trees, the UCTSS demonstrated higher average droplet density and droplet deposition at the middle levels, where the distance to the UCTSS nozzle is the shortest during spraying.

Considering the overall coefficient of variation (CV) of droplet density and droplet deposition in Table 5, the UCTSS exhibited a smaller overall CV compared to the T50. However, when comparing the CV at the same levels, some were higher for the UCTSS than for the T50. This phenomenon can be attributed to the use of an arc-shaped spray boom in the UCTSS, which results in better atomization and higher overall uniformity. Nevertheless, during the spraying process, the UCTSS UAV completes only one pass from top to bottom. Its adaptability to trees with irregular

shapes is relatively poor. Thus, the advantage of the UCTSS is mainly reflected in spraying taller trees in standard orchards, and improvements are needed for uniform spraying on trees of varying shapes.

This paper compares the spraying effectiveness of the UCTSS with that of the DJI-T50, primarily to validate the feasibility of the UCTSS and highlight its advantages over single UAV spraying. The DJI-T50, a leading model in the orchard protection industry with proven market effectiveness, was selected for this comparison. In addition to the earlier analyses, the DJI-T50 demonstrates a faster spraying operation than the UCTSS, which is one of its key advantages. Following the validation of the UCTSS's feasibility, the next step involves further optimizing the system. The ultimate goal is to enable the UAV within the UCTSS to carry a spray boom, akin to a human hand, allowing for targeted and shape-conforming spraying based on the external contours of the fruit trees. Simultaneously, the UGV will function like the human body, transporting heavy equipment such as the pesticide tank. Finally, by integrating LiDAR and computer vision methods to mimic the human eye, the system aims to gather information about the position, size, and external contours of the fruit trees, thereby enhancing the capability for shape-conforming targeted spraying.

Table 5 Comparison of coefficient of variation

Value	Position	Spraying method	1			2			3			Average
			Upper	Middle	Lower	Upper	Middle	Lower	Upper	Middle	Lower	
Droplet density	Leaf surface	UCTSS	64.26%	10.79%	39.13%	44.86%	59.92%	37.00%	48.26%	20.82%	71.89%	56.16%
				59.32%			60.39%			48.76%		
		DJI-T50	71.93%	105.47%	81.62%	103.07%	110.39%	149.24%	91.67%	87.26%	75.08%	102.88%
				108.01%			115.27%			85.37%		
	Leaf underside	UCTSS	38.94%	71.32%	84.01%	56.67%	54.78%	88.55%	39.64%	61.14%	49.37%	69.99%
				78.99%			79.80%			51.19%		
		DJI-T50	87.51%	145.11%	120.39%	100.85%	157.91%	132.69%	89.61%	136.96%	80.35%	122.40%
				132.37%			127.87%			106.95%		
Droplet deposition	Leaf surface	UCTSS	130.40%	8.17%	53.31%	60.71%	65.90%	65.96%	59.34%	41.29%	133.36%	82.04%
				76.01%			78.94%			91.16%		
		DJI-T50	63.35%	135.74%	126.49%	99.36%	85.90%	161.32%	93.00%	79.05%	58.44%	101.85%
				121.73%			109.49%			74.32%		
	Leaf underside	UCTSS	95.00%	181.52%	120.50%	99.65%	119.62%	85.35%	58.96%	24.26%	70.30%	124.43%
				222.71%			100.81%			49.76%		
		DJI-T50	101.79%	126.65%	123.99%	110.76%	177.82%	134.54%	95.00%	223.61%	91.35%	138.47%
				123.79%			153.00%			138.63%		

4 Conclusions

The main contributions of this paper are summarized as follows:

(1) For standard orchards with taller fruit trees and denser canopies, a UAV-UGV cooperative targeted spraying system (UCTSS) was proposed. Based on ROS networking, a prototype was constructed that includes one UAV, one UGV, and spraying equipment.

(2) The UAV-UGV formation algorithm was designed for controlling the movement of the UCTSS and developed a targeted spraying detection method for detecting fruit tree positions and spraying within the system. Separate tests were conducted to verify the feasibility of each individual task.

(3) Experiments were conducted in the Jinggang pomelo orchard. The results showed that the average tracking error of the UAV during formation movement was 0.158 m and the standard deviation was 0.048 m, which met the stability requirements for movement. The average tracking error during the spraying stage was 0.013 m and the standard deviation was 0.032 m, which met the accuracy requirements for the spraying phase. In terms of spraying effectiveness, the UCTSS exhibited higher average droplet density and deposition on each layer of the fruit tree compared to the DJI-T50. Additionally, the UCTSS demonstrated lower coefficients of variation between layers, indicating an improvement for overall spraying uniformity, thereby verifying the feasibility of the proposed UCTSS in this paper.

The UCTSS proposed in this paper has identified several issues during practical experiments and usage that will be addressed in future work:

(1) Regarding targeted spraying, the system achieved targeted spraying in the E-N coordinate system but did not accomplish real-time height-adaptive targeted spraying for each tree in the vertical direction. Therefore, it is only suitable for standard orchards with trees of similar heights.

(2) The method used in this paper to detect tree positions with LiDAR requires re-calibration of relevant thresholds when there are significant changes in the tree dimensions or row spacing. While this method has low costs, it lacks a high level of intelligence.

(3) The UCTSS proposed in this paper currently only performs single-pass spraying from the side of fruit trees, moving from top to bottom. The spray width can be adjusted by manually changing the length of the spray boom; however, for fruit trees with a crown width exceeding 3.2 m, a UAV with a greater payload capacity will be required.

In future work, the integration of LiDAR and computer vision will be pursued to detect the precise positions and detailed dimensions of fruit trees. This enhanced sensing capability will enable more accurate control of the movement of the UAV and UGV, particularly in adapting to height variations for targeted spraying. Additionally, the trajectory planning for UAV during the spraying process will be redesigned to make it adaptable to fruit trees with different contours and heights. This approach aims to address the previously mentioned issues, ultimately improving the adaptability and precision of the UCTSS for targeted spraying. In the experiments of this paper, the focus was on validating the feasibility of the UCTSS. After refining the aforementioned work, further optimization of parameters, including spray pressure and

UAV speed during spraying, and the addition of parameters such as droplet diameter, will be conducted to provide a more comprehensive evaluation criterion.

Acknowledgements

This work was supported by Science and Technology Plan of Ji' an City of China (Grant No. 20211-055316 and [2020]83), and in part by the Laboratory of Lingnan Modern Agriculture Project (Grant No. NT2021009), Science and Technology Plan of Guangdong Province of China (Grant No. 2023B10564002), and China Scholarship Council (Grant No. 202308440394). The authors would like to express special gratitude to Benniu Ecological Farm for providing the test field, and to Jinggang Pomelo Standardization Demonstration Base for providing the experimental site and the use of the DJI-T50 mentioned in this paper.

[References]

[1] Li L L, He X K, Song J L, Liu Y, Wang Z C, Li J Y, et al. Comparative experiment on profile variable rate spray and conventional air assisted spray in orchards. Transactions of the CSAE, 2017; 33(16): 56–63. (in Chinese)

[2] Ding S M, Fu X M, Xue X Y, Zhou L F, Lü X L. Design and experiment of self-propelled air-assisted sprayer in orchard with dwarf culture. Transactions of the CSAE, 2013; 29(15): 18–25. (in Chinese)

[3] Jiang H H, Niu C Q, Liu L M, Wang D W, Wang J S, Mao W H. Design and experiment of air volume control system of orchard multi-pipe air sprayer. Transactions of the CSAM, 2020; 51(S2): 298–307. (in Chinese)

[4] Qiu W, Gu J B, Ding W M, Lü X L, Sun C D, Lu J. Experiment on control effect of different pesticide concentration using air-assisted sprayer. Journal of Chinese Agricultural Mechanization, 2015; 46(1): 94–99. (in Chinese)

[5] Li T, Qi P, Wang Z C, Xu S Q, Huang Z, Han L, et al. Evaluation of the effects of airflow distribution patterns on deposit coverage and spray penetration in multi-unit air-assisted sprayer. Agronomy, 2022; 12(4): 944.

[6] Ru Y, Zhou H P, Jia Z C, Wu X W, Fan Q N. Design and application of electrostatic spraying system. Journal of Nanjing Forestry University: Natural Sciences Edition, 2011; 35(1): 91–94. (in Chinese)

[7] He X K, Yan K R, Chu J Y, Wang J, Zeng A J. Design and testing of the automatic target detecting, electrostatic, air assisted, orchard sprayer. Transactions of the CSAE, 2003; 19(6): 78–80. (in Chinese)

[8] Yang Z, Niu M M, Li J, Xing X, Xu J T, Chen Z C. Design and experiment of an electrostatic sprayer with on-line mixing system for orchard. Transactions of the CSAE, 2015; 31(21): 60–67. (in Chinese)

[9] Qiu W, Sun H, Sun Y H, Liao Y Y, Zhou L F, Wen Z J. Design and test of circulating air-assisted sprayer for dwarfed orchard. Transactions of the CSAE, 2021; 37(6): 18–25. (in Chinese)

[10] Niu M M, Fang H M, Qiao L, Jian S C, Zhu Z B, Peng Q J. Design and experiment of high clearance type recycling tunnel sprayer. Journal of Chinese Agricultural Mechanization, 2019; 40(11): 41–48. (in Chinese)

[11] Li L F, He X, Xiao Y M, Jiao T W, Li W. Design and experimental verification of targeted and variable sprayer for the potato. Agriculture, 2023; 13(4): 797.

[12] Li L L, He X K, Song J L, Wang X N, Jia X M, Liu C H. Design and experiment of automatic profiling orchard sprayer based on variable air volume and flow rate. Transactions of the CSAE, 2017; 33(1): 70–76. (in Chinese)

[13] Song S R, Ruan Y C, Hong T S, Dai Q F, Zhang C. Self-adjustable fuzzy PID control for solution pressure of pipeline spray system in orchard. Transactions of the CSAE, 2011; 27(6): 157–161. (in Chinese)

[14] Arshed A, Shahram H, Naveed T M, Rashid S S, Rashed A. A performance comparison of variable rate technologies for spot-specific and uniform spraying for citrus orchard. Environmental Sciences Proceedings, 2022; 23(1): 21.

[15] Xiao K, Hao Y, Gao G D. Design and experiment of automatic variable-distance precision spraying system in orchard. Transactions of the CSAM, 2022; 53(10): 137–145. (in Chinese)

[16] Chen Z W, Hu Z R, Xiong Y F, Wang P, Yu Y, Peng M, et al. Design and test of the canopy wrap-around profiling-to-target sprayer for orchards. Transactions of the CSAE, 2023; 39(3): 23–32. (in Chinese)

[17] Zhou Z Y, Ming R, Zang Y, He X G, Luo X W, Lan Y B. Development status and countermeasures of agricultural aviation in China. Transactions of the CSAE, 2017; 33(20): 1–13. (in Chinese)

[18] Daly J M, Ma Y, Waslander S L. Coordinated landing of a quadrotor on a skid-steered ground vehicle in the presence of time delays. Autonomous Robots, 2015; 38(2): 179–191.

[19] Rodriguez-Ramos A, Sampedro C, Bavle H, Moreno I G, Campoy P. A deep reinforcement learning technique for vision-based autonomous multirotor landing on a moving platform: RSJ International Conference on Intelligent Robots and Systems (IROS), IEEE, 2018; pp.1010–1017. DOI:10.1109/IROS.2018.8594472

[20] Lange S, Sunderhauf N, Protzel P. A vision based onboard approach for landing and position control of an autonomous multirotor UAV in GPS-denied environments. 14th International Conference on Advanced Robotics, IEEE, 2009; pp.484-961.

[21] Yang T, Ren Q, Zhang F B, Xie B L, Ren H L, Li J, et al. Hybrid camera array-based UAV auto-landing on moving UGV in GPS-denied environment. Remote Sensing, 2018; 10(11): 1829.

[22] Li Y F, Han L, Liu L M, Huang Z, Wang C L, He X K. Design and spray performance evaluation of an air–ground cooperation stereoscopic plant protection system for mango orchards. Agronomy, 2023; 13(8): 2007.

[23] Tokekar P, Hook J V, Mulla D, Isler V. Sensor planning for a symbiotic UAV and UGV system for precision agriculture. IEEE Transactions on Robotics, 2016; 32(6): 1498–1511.

[24] Zhang M, Li S R, Li B Q. An air-ground cooperative scheduling model considering traffic environment and helicopter performance. Computers & Industrial Engineering, 2021; 158(4): 107458.

[25] Godbole A R, Subbarao K. Nonlinear control of unmanned aerial vehicles with cable suspended payloads. Aerospace Science and Technology, 2019; 93: 105299.

[26] Zhang J L, Yan J G, Zhang P. Multi-UAV formation forming control based on adaptive method under wind field disturbances. Acta Aeronautica ET Astronautica Sinica, 2020; 41(1): 229–242. (in Chinese)

[27] Wu Y, Liang T J. Improved consensus-based algorithm for unmanned aerial vehicle formation control. Acta Aeronautica ET Astronautica Sinica, 2020; 41(9): 167–185. (in Chinese)

[28] Chen Z W, Xiong Y F, Hu Z R, Li C, Pang Y L, Yang M J. Path finding and tracking of clutch brake track chassis based on virtual searchlight. Transactions of the CSAE, 2023; 39(12): 10–19. (in Chinese)

[29] Jiang S J, Ma H T, Yang S H, Zhang C, Su D B, Zheng Y J, et al. Target detection and tracking system for orchard spraying robots. Transactions of the CSAE, 2021; 37(9): 31–39. (in Chinese)

[30] Song S R, Chen J Z, Hong T S, Zhang C, Dai Q F, Xue X Y. Design and experiment of orchard flexible targeted spray device. Transactions of the CSAE, 2015; 31(10): 57–63. (in Chinese)

[31] Sultan M M, Zahid A, He L, Choi D, Krawczyk G, Zhu H P, et al. Development of a LiDAR-guided section-based tree canopy density measurement system for precision spray applications. Computers and Electronics in Agriculture, 2021; 182: 106053.

[32] Aljaž O, Tone G, Marko H, Brane Š, Matej S. Real-time positioning algorithm for variable-geometry air-assisted orchard sprayer. Computers and Electronics in Agriculture, 2013; 98: 175–182.

[33] Zhou L F, Xue X Y, Zhou L X, Zhang L, Ding S M, Chang C, et al. Research situation and progress analysis on orchard variable rate spraying technology. Transactions of the CSAE, 2017; 33(23): 80–92. (in Chinese)

[34] Lin Z, Fan X L, Deng K H, Lin J Q, Zhou Z Y. Influence of plant protection unmanned aircraft operation parameters and operation mode on the effectiveness of controlling Panonychus citri mite in Jinggang Honeydew. Journal of Environmental Entomology, 2024: https://link.cnki.net/urlid/44.1640.Q.20240703.1156.002. (in Chinese)